



Published in final edited form as:

Nature. 2017 November 02; 551(7678): 115–118. doi:10.1038/nature24057.

Glucose feeds the TCA cycle via circulating lactate

Sheng Hui^{1,2}, Jonathan M. Ghergurovich^{1,3}, Raphael J. Morscher^{1,2}, Cholsoon Jang^{1,2}, Xin Teng^{1,2}, Wenyun Lu^{1,2}, Lourdes A. Esparza⁴, Tannishtha Reya⁴, Le Zhan^{5,6}, Jessie Yanxiang Guo^{5,7,8}, Eileen White^{5,6}, and Joshua D. Rabinowitz^{1,2,5}

¹Lewis-Sigler Institute for Integrative Genomics, Princeton University, Princeton, New Jersey 08544, USA

²Department of Chemistry, Princeton University, Princeton, New Jersey 08544, USA

³Department of Molecular Biology, Princeton University, Princeton, New Jersey 08544, USA

⁴Departments of Pharmacology and Medicine, Moores Cancer Center, University of California San Diego School of Medicine, La Jolla, California 92093, USA

⁵Rutgers Cancer Institute of New Jersey, New Brunswick, New Jersey 08903, USA

⁶Department of Molecular Biology and Biochemistry, Rutgers University, Piscataway, New Jersey, 08854, USA

⁷Department of Medicine, Rutgers Robert Wood Johnson Medical School, New Brunswick, New Jersey 08901, USA

⁸Department of Chemical Biology, Rutgers Ernest Mario School of Pharmacy, Piscataway, New Jersey 08854, USA

Abstract

Mammalian tissues are fuelled by circulating nutrients, including glucose, amino acids, and various intermediary metabolites. Under aerobic conditions, glucose is generally assumed to be burned fully by tissues via the tricarboxylic acid cycle (TCA cycle) to carbon dioxide.

Alternatively, glucose can be catabolized anaerobically via glycolysis to lactate, which is itself also a potential nutrient for tissues¹ and tumours^{2–5}. The quantitative relevance of circulating

Reprints and permissions information is available at www.nature.com/reprints.

Correspondence and requests for materials should be addressed to J.D.R. (joshr@princeton.edu).

Online Content Methods, along with any additional Extended Data display items and Source Data, are available in the online version of the paper; references unique to these sections appear only in the online paper.

Supplementary Information is available in the online version of the paper.

Author Contributions

S.H., R.J.M., and J.D.R. came up with the general approach. S.H., J.M.G., R.J.M., and C.J. designed and performed the wild-type mouse isotope tracing studies. J.M.G., L.A.E., and T.R. designed and performed the pancreatic cancer GEMM studies. X.T., L.Z., J.Y.G., and E.W. designed and performed the lung cancer GEMM studies. W.L. performed LC–MS analysis. S.H. and J.D.R. developed the mathematical models. S.H. and J.D.R. wrote the paper with help from all authors.

Author Information The authors declare no competing financial interests. Readers are welcome to comment on the online version of the paper.

Publisher's note: Springer Nature remains neutral with regard to jurisdictional claims in published maps and institutional affiliations.

Reviewer Information *Nature* thanks S. Kempa, M. Yuneeva and the other anonymous reviewer(s) for their contribution to the peer review of this work.

lactate or other metabolic intermediates as fuels remains unclear. Here we systematically examine the fluxes of circulating metabolites in mice, and find that lactate can be a primary source of carbon for the TCA cycle and thus of energy. Intravenous infusions of ^{13}C -labelled nutrients reveal that, on a molar basis, the circulatory turnover flux of lactate is the highest of all metabolites and exceeds that of glucose by 1.1-fold in fed mice and 2.5-fold in fasting mice; lactate is made primarily from glucose but also from other sources. In both fed and fasted mice, ^{13}C -lactate extensively labels TCA cycle intermediates in all tissues. Quantitative analysis reveals that during the fasted state, the contribution of glucose to tissue TCA metabolism is primarily indirect (via circulating lactate) in all tissues except the brain. In genetically engineered lung and pancreatic cancer tumours in fasted mice, the contribution of circulating lactate to TCA cycle intermediates exceeds that of glucose, with glutamine making a larger contribution than lactate in pancreatic cancer. Thus, glycolysis and the TCA cycle are uncoupled at the level of lactate, which is a primary circulating TCA substrate in most tissues and tumours.

Mammals generate energy by catabolizing food into carbon dioxide (CO_2). Glucose is generally assumed to be catabolized in cells via the concerted action of glycolysis and the TCA cycle. Cells and tissues can also share metabolic tasks by exchanging intermediary metabolites, such as lactate. Here we systematically investigate the significance of different circulating metabolic intermediates. The circulatory turnover flux (F_{circ}) of a given metabolite refers to the rate at which tissues collectively consume the metabolite from the arterial circulation (F_c) and produce and excrete the metabolite into the venous circulation (F_p) (Fig. 1a), with these two rates being equal at steady state. We considered whether there is any fundamental limit on which metabolites can have high F_{circ} (that is, can contribute substantially to inter-organ fluxes). For metabolite M , its consumption by the tissues cannot occur faster than the rate at which it is pumped from the heart:

$$F_{\text{circ}} \leq \text{cardiac output} \times [M] \quad (1)$$

Thus, only metabolites that are reasonably concentrated in blood can contribute substantially to inter-organ fluxes, with 39 metabolites in mice having a sufficient concentration (greater than $30 \mu\text{M}$) to potentially have greater than 10% of the F_{circ} of glucose⁶ (Extended Data Fig. 1).

We measured F_{circ} for most of these species following an approach classically used to measure whole-body glucose production flux⁷: for each metabolite M , a trace amount of ^{13}C -labelled M is infused into the circulation at a constant rate R until steady-state labelling is achieved (Fig. 1b,c), at which point the labelled fraction L is related to the turnover flux as:

$$F_{\text{circ}} = \frac{R(1-L)}{L} \quad (2)$$

For derivation, see Supplementary Note 1. Infusions were into the right jugular vein of freely moving C57BL/6 mice that spectrometry (LC-MS). Despite glucose being widely assumed

to be the predominant circulating chad been fasted for 8 h (Extended Data Fig. 2a), with measurements of serum labelling via liquid chromatography–mass carbon source, on a molar basis, lactate showed a 2.5-fold higher circulatory turnover flux (1.25-fold higher on a per-carbon-atom basis) (Fig. 1d and Extended Data Fig. 2b–d). The other metabolites with substantial circulatory turnover fluxes (greater than 20% of glucose on a molar basis) were pyruvate, glycerol, acetate, 3-hydroxybutyrate, alanine and glutamine, each of which had a turnover flux less than 20% that of lactate (Table 1). F_{circ} of free palmitate was 15% that of glucose on a molar basis, which equals 40% on a carbon atom basis. Essential amino acids, which are not biosynthesized and come from either diet or tissue protein degradation, exhibited lower F_{circ} values, which were proportional to the abundances of the amino acids in protein (Fig. 1e). Like lactate, infused pyruvate was rapidly consumed by tissues, but its circulating concentration is too low to carry comparable flux (equation (1) and Supplementary Note 1).

Previous F_{circ} measurements have been largely restricted to glucose. However measurements have been reported for lactate and, consistent with our data, showed lactate turnover flux in excess of glucose turnover flux^{8–11}. The physiological significance of these measurements has generally been dismissed, on the basis of the assumption that high lactate turnover flux merely reflects rapid lactate-pyruvate exchange. In actuality, such exchange does not change the ¹³C-labelling pattern of lactate and therefore does not contribute to turnover flux. Rather, the measured lactate circulatory turnover flux reflects the whole-body pyruvate production rate, multiplied by the fraction of tissue pyruvate that is excreted into the circulation as lactate (Supplementary Note 2 and Extended Data Fig. 3a). Thus, high lactate F_{circ} reflects a high fraction of tissue pyruvate being excreted as lactate (and a high fraction of tissue pyruvate being derived from circulating lactate).

Another concern with regards to prior measurements is differences in arterial and venous lactate labelling^{12–16}. We modelled the origin of such differences using partial differential equations to examine labelling across a tissue capillary bed (Supplementary Note 1 and Extended Data Fig. 3b). We find that the difference in arterial and venous labelling ($L_a - L_v = \Delta L$) depends on the relative magnitude of F_{circ} compared to metabolite flow:

$$\frac{\Delta L}{L_a} = \frac{F_{\text{circ}}}{\text{cardiac output} \times [M]} \quad (3)$$

In cases of substantial ΔL , F_{circ} can be determined by equation (3) or by equation (2) with L the arterial metabolite labelling, with similar results (Supplementary Note 1). Thus, rather than precluding accurate determination of F_{circ} , the arterial–venous difference in lactate labelling (Extended Data Fig. 3c) confirms the high circulatory turnover flux of lactate.

To test the hypothesis that lactate is a primary circulating carbon carrier, we examined tissue metabolite labelling after infusing uniformly ¹³C-labelled forms of the two primary carbon sources in cell culture (glucose and glutamine) or lactate. At steady state (Extended Data Fig. 4), the normalized labelling of a tissue metabolite from a circulating nutrient ($L_{\text{metabolite} \leftarrow \text{nutrient}}$) is defined as the fraction of ¹³C atoms in the metabolite, normalized to

the fraction of ^{13}C atoms in the circulating nutrient^{17–19}. As expected, normalized labelling of glycolytic and pentose phosphate intermediates in tissue was greatest from the glucose infusion, whereas tissue lactate was labelled substantially from both glucose and lactate tracer infusions (Extended Data Fig. 5). In most tissues, normalized labelling of TCA intermediates, as represented by malate and succinate (Extended Data Fig. 6), was greatest from the lactate infusion (Fig. 2a–c).

Although normalized TCA labelling from lactate ($L_{\text{TCA}\leftarrow\text{lac}}$) generally exceeded that from glucose ($L_{\text{TCA}\leftarrow\text{glc}}$), the difference was, on average, modest (approximately 30% versus approximately 20%). A substantial fraction of serum lactate was, however, derived from glucose (red bar in Fig. 2b). We denote the fraction of ^{13}C atoms in serum lactate following labelled glucose infusion, normalized to the fraction of ^{13}C atoms in serum glucose, as $L_{\text{lac}\leftarrow\text{glc}}$. Measurement of $L_{\text{TCA}\leftarrow\text{lac}}$ and $L_{\text{lac}\leftarrow\text{glc}}$ allows us to determine quantitatively how much of the TCA labelling from labelled glucose infusion actually arises through labelled circulating lactate ($L_{\text{TCA}\leftarrow\text{lac}} \cdot L_{\text{lac}\leftarrow\text{glc}}$). This amount is shown as the solid line in Fig. 2d. Within the margins of error, TCA labelling from glucose is fully accounted for by labelling through circulating lactate in every tissue except for the brain.

Analogously, labelled lactate infusion contributes to TCA labelling through labelled circulating glucose produced by gluconeogenesis ($L_{\text{TCA}\leftarrow\text{glc}} \cdot L_{\text{glc}\leftarrow\text{lac}}$, dashed line in Fig. 2d). To quantitatively delineate the direct flux contributions to the TCA cycle by circulating glucose, lactate, and glutamine, we developed a linear algebra model to compute the direct TCA substrate usage of individual tissues (Fig. 2e and Supplementary Note 3). This analysis confirmed that, except in the brain, direct glucose flux to the TCA cycle is close to zero in fasted mice. Glutamine and lactate together account for about half of TCA cycle carbon. It is likely that most of the remainder comes from a combination of other amino acids and fat. Thus, in the fasted state, glucose feeds the TCA cycle mainly via circulating lactate in all tissues but the brain.

At the whole-body level, the circulatory turnover fluxes of glucose and lactate and their overall interconversion in body tissue can be quantitatively accounted for by a steady-state flux balance model (Supplementary Note 4), with fluxes determined solely on the basis of labelling of circulating glucose and lactate. In fasting mice, modelling revealed that the majority of glucose enters the TCA via circulating lactate (Fig. 2f). Similar relative contributions of glucose and lactate were also observed in anaesthetized mice (Extended Data Fig. 7).

We next examined fluxes of glucose and lactate in fed mice, where insulin signalling could increase tissue glucose metabolism. Indeed, F_{circ} for glucose was 3.1-fold higher than in fasted mice. This was accompanied by a small increase in F_{circ} for lactate, which was about 1.1-fold of F_{circ} for glucose on a molar basis (55% on a per-carbon-atom basis) (Fig. 3a). TCA labelling from glucose also increased (Extended Data Fig. 8), with glucose and lactate making a roughly equal direct contribution to the muscle TCA cycle. In other organs, even in the fed state, glucose contributes to the TCA cycle mostly through circulating lactate (Fig. 3b, c). Quantitative whole-body modelling showed that, in the fed state, about 40% of glucose feeds the TCA cycle through circulating lactate (Fig. 3d and Supplementary Note 4).

Further work is required to assess other states, such as exercise, and to identify the tissue compartments responsible for glucose-to-lactate flux.

Rapid glucose catabolism to lactate was the first molecular phenotype assigned to cancer^{20,21}. Tumours are often thought of as having an isolated metabolic microenvironment owing to poor perfusion, in which local exchange of nutrients (for example, between cancer cells and stromal cells) predominates over nutrient exchange with the circulation. We measured TCA substrate contributions in three genetically engineered mouse models (GEMMs). Notably, in all three cases, the contribution of circulating lactate to tumour TCA intermediates exceeded that of glucose by about twofold (Fig. 4a–c), with quantitative analysis consistent with glucose contributing to the tumour TCA cycle only through circulating lactate (Extended Data Fig. 9). Thus, the GEMM tumours that we studied are thoroughly perfused by lactate. This does not rule out the potential for some sections within human tumours to be less well perfused⁵ or for an important subset of tumour cells to be isolated within a poorly perfused metabolic niche. Note that in normal lung tissue and lung cancer, the largest TCA contribution was from lactate, whereas in the pancreas and pancreatic cancer, glutamine contributed more (Figs 2e and 4d), consistent with tumours mirroring the substrate preferences of their tissues of origin^{22,23}.

It is useful to differentiate between the above conclusions that arise directly from experimental data and those that are inferred on the basis of quantitative modelling, which omits certain biological complexity, such as tissue heterogeneity. The experimental data demonstrate that circulating lactate is a major source of TCA intermediates. The quantitative modelling leads to the additional conclusion that, in most tissues and GEMM tumours, the contribution of glucose to the TCA cycle is mostly through circulating lactate.

The metabolic role of lactate is well recognized, including as a fuel for tissues²⁴ and tumours^{2–5,25}. In the classical Cori cycle, muscle produces lactate which is then taken up by the liver for gluconeogenesis. Previous work has highlighted the potential for lactate to shuttle carbon both between and within tissues^{26–29}. We find that such shuttling underlies the majority of circulating lactate turnover, with glucose feeding TCA metabolism mainly through circulating lactate (Fig. 4e). This picture requires high lactate dehydrogenase (LDH) activity and rapid lactate transport across the plasma membrane. Mammals encode two ubiquitously expressed LDH isozymes (LDHA and LDHB), as well as four monocarboxylate transporters (MCT1–MCT4). While the different isozymes show some kinetic differences, the direction of net flux is determined by thermodynamics. Genetic manipulation of these enzymes and transporters will be important to establish the biochemical basis of the phenomena reported here.

Among the many metabolic intermediates, why does lactate carry high flux? Lactate is redox-balanced with glucose. The rapid exchange of both tissue lactate and pyruvate with the circulation may help to equate cytosolic NAD⁺/NADH ratios across tissues, allowing the whole body to buffer NAD(H) disturbances in any given location³⁰. Nearly complete lactate sharing between tissues effectively decouples glycolysis and the TCA cycle in individual tissues, allowing independent tissue-specific regulation of both processes. Because almost all ATP is made in the TCA cycle, each tissue can acquire energy from the largest dietary

calorie constituent (carbohydrate) without needing to carry out glycolysis. In turn, glycolytic activity can be modulated to support cell proliferation, NADPH production by the pentose phosphate pathway, brain activity, and systemic glucose homeostasis²¹. In essence, by having glucose feed the TCA cycle via circulating lactate, the housekeeping function of ATP production is decoupled from glucose catabolism. In turn, glucose metabolism is regulated to serve more advanced objectives of the organism.

METHODS

Data reporting

No statistical methods were used to predetermine sample size. The experiments were not randomized.

Intravenous infusion of wild-type C57BL/6 mice

Animal studies followed protocols approved by the Princeton University Institutional Animal Care and Use Committee. *In vivo* infusions were performed on 12–14-week-old C57BL/6 mice pre-catheterized in the right jugular vein (Charles River Laboratories). Mice were randomly chosen for infusions of different tracers. No blinding was performed. A minimum of three mice was used for each tracer. To collect arterial blood samples, we used mice pre-catheterized in both the right jugular vein and left carotid artery (Charles River Laboratories), infusing through the venous catheter and drawing blood from the arterial catheter. Venous samples were taken from tail bleeds. The mice were on a normal light cycle (8:00–20:00). On the day of the infusion experiment, mice were transferred to new cages without food around 8:00 (beginning of their sleep cycle) and infused for 2.5 h starting at around 14:00. To analyse the fed state, the mice were maintained without food until around 19:00, at which time chow was placed back in the cages and the 2.5 h infusion initiated. The mouse infusion setup (Instech Laboratories) included a tether and swivel system so that the animal had free movement in the cage. Water-soluble isotope-labelled metabolites (Cambridge Isotope Laboratories) were prepared as solutions in sterile normal saline and infused via the catheter at a constant rate for 2.5 h (unless otherwise indicated). To make ¹³C-palmitate solution, [U-¹³C]sodium palmitate was complexed with bovine serum albumin in a 2:1 molar ratio³¹. Detailed infusion parameters are listed in Supplementary Table 1. Blood samples (~20 µl) were placed on ice in the absence of anticoagulant, and centrifuged at 4 °C to isolate serum. At the end of the infusion, the mouse was euthanized by cervical dislocation and tissues were quickly dissected and snap frozen in liquid nitrogen with pre-cooled Wollenberger clamp³². Serum and tissue samples were kept at –80 °C until LC–MS or GC–MS analysis.

Intravenous infusion of genetically engineered mouse models

Animal studies with the lung cancer GEMMs followed protocols approved by the Rutgers University Institutional Animal Care and Use Committee. *Kras*^{LSL-G12D/+} *Trp53*^{flox/flox} (KP) and *Kras*^{LSL-G12D/+} *Stk11*^{flox/flox} (*Stk11* is also known as *Lkb1* and the mouse model is referred to as the KL lung cancer model) mice were intranasally infected with recombinant, replication-deficient adenovirus expressing Cre recombinase (University of Iowa Adenoviral Core) at 4×10^7 plaque-forming units per mouse at 6–8 weeks of age. At 12 weeks post-

infection, catheters were surgically implanted into the right jugular vein of KP and KL GEMMs and [U-¹³C]glucose (0.2 M, 0.1 μl g⁻¹ min⁻¹), [U-¹³C]glutamine (0.1 M, 0.1 μl g⁻¹ min⁻¹), or [U-¹³C] sodium lactate (5% w/w, 0.1 μl g⁻¹ min⁻¹) was infused into 8-h fasted mice for 2.5 h. Blood samples were collected from the tail vein and facial vein for measurement of serum enrichment of isotopic tracers. Mice were euthanized by cervical dislocation and tumours were quickly snap frozen in liquid nitrogen using a pre-cooled Wollenberger clamp. Throughout the experiments, mice were examined for evidence of distress due to lung tumour progression (for example, difficulty breathing, difficulty moving, significant weight loss, or moribund status) every day to ensure the health and well-being of the animal. Any animals exhibiting signs of distress would have been euthanized. At the time of *in vivo* infusion, none of the mice showed signs of distress.

Animal studies with the pancreatic cancer GEMM followed protocols approved by the University of California at San Diego Institutional Animal Care and Use Committee. *Kras^{LSL-G12D/+}Trp53^{flox/flox}Ptf1a^{CRE/+}* (KP^{f/f}C) mice were used. While *Kras* mutation alone leads to PanIN formation³³, when combined with deletion of *Trp53* it drives progression to adenocarcinoma³⁴. At ~10 weeks old, catheters were surgically implanted into the right jugular vein of KP^{f/f}C mice and [U-¹³C]glucose (0.2 M, 0.1 μl g⁻¹ min⁻¹), [U-¹³C]glutamine (0.1 M, 0.1 μl g⁻¹ min⁻¹), or [U-¹³C] sodium lactate (5% w/w, 0.1 μl g⁻¹ min⁻¹) was infused into 8-h fasted mice for 2.5 h. Blood samples were collected from the tail vein for measurement of serum enrichment of isotopic tracers. Mice were euthanized by cervical dislocation, and tumours were quickly snap frozen in liquid nitrogen using a pre-cooled Wollenberger clamp. Throughout the experiments, tumour progression was monitored according to protocols approved by the University of California San Diego Institutional Animal Care and Use Committee: weekly (for no visible, palpable, clinical, or behavioural signs of tumour burden), twice weekly (for visible or palpable tumours; changes in appearance or behaviour), and/or daily (for any signs of morbidity or mortality). It is important to note that with our pancreatic cancer model, in most instances, the mice show no visible signs of disease—no palpable tumour, no lethargy, no hunching, no weight loss, although we monitored carefully for these signs of distress.

Metabolite measurement

Metabolites were extracted from serum samples (thawed on ice) by adding 65 μl 80:20 methanol:water solution at -80 °C to 5 μl of serum sample, followed by vortexing for 10 s, incubation at 4 °C for 10 min, and centrifugation at 4 °C and 16,000g for 10 min. To extract metabolites from tissue samples, frozen tissue samples were first weighed (~20 mg each sample) and ground using a Cryomill (Retsch). The resulting powder was then mixed with -20 °C 40:40:20 methanol:acetonitrile:water solution, followed by vortexing for 10 s, incubation at 4 °C for 10 min, and centrifugation at 4 °C and 16,000g for 10 min. The volume of the extraction solution (in μl) was 40 × the weight of tissue (in mg). The supernatant was transferred to LC-MS autosampler vials for analysis.

Serum and tissue extracts were analysed using LC-MS. In brief, a quadrupoleorbitrap mass spectrometer (Q Exactive Plus, Thermo Fisher Scientific) operating in negative ion mode was coupled to hydrophilic interaction chromatography via electrospray ionization and used

to scan from m/z 73 to 1,000 at 1 Hz and 140,000 resolution. LC separation was achieved on a XBridge BEH Amide column (2.1 mm \times 150 mm, 2.5 μ m particle size, 130 Å pore size; Waters) using a gradient of solvent A (20 mM ammonium acetate + 20mM ammonium hydroxide in 95:5 water:acetonitrile, pH 9.45) and solvent B (acetonitrile). Flow rate was 150 μ l min⁻¹. The gradient was: 0 min, 85% B; 2 min, 85% B; 3 min, 80% B; 5 min, 80% B; 6 min, 75% B; 7 min, 75% B; 8 min, 70% B; 9 min, 70% B; 10 min, 50% B; 12 min, 50% B; 13 min, 25% B; 16 min, 25% B; 18 min, 0% B; 23 min, 0% B; 24 min, 85% B; 30 min, 85% B. Data were analysed using the MAVEN software³⁵. Isotope labelling was corrected for natural abundances of ¹³C, ²H, and ¹⁵N. Circulating glycerol labelling was determined by first converting serum glycerol to glycerol-3-phosphate using glycerol kinase and then measuring the labelling of glycerol-3-phosphate with LC-MS.

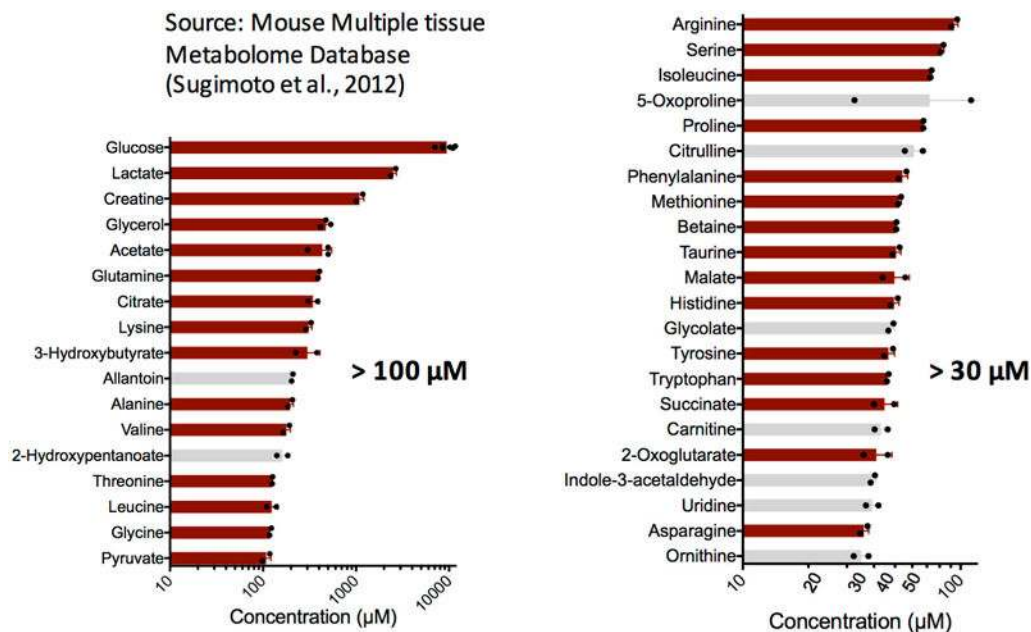
For acetate, circulating metabolite labelling was determined by GC-MS using a 7890A GC system coupled to a 5975 MSD mass spectrometer (Agilent) after derivatization with 2,3,4,5,6-pentafluorobenzyl bromide as described³⁶. GC separation was achieved using an Agilent J&W 122-7033 column (30 m \times 0.25 mm \times 0.5 μ m). The GC temperature program was: 0 min, 35 °C; 6 min, 35 °C; 12 min, 220 °C; 17 min, 220 °C, followed by returning to 35 °C for the next injection. Other GC parameters were: injection volume 1 μ l; He as carrier gas at a flow rate of 1.2 ml min⁻¹; inlet temperature 250 °C; transfer line temperature 280 °C. Mass spectrometry detection was in electron impact ionization mode, with SIM scans of m/z 240.3 and 242.3 for unlabelled and ¹³C₂-acetate, respectively.

Free fatty acids in serum samples (thawed on ice) were extracted by adding 200 μ l ethyl acetate at room temperature to 10 μ l serum samples, followed by vortexing for 10 s, incubation at 4 °C for 10 min, and centrifugation at 16,000g for 10 min. The top layer of approximately 190 μ l was transferred to a new glass vial before being dried under nitrogen gas flow. The dried extract was dissolved in 100 μ l 1:1 isopropanol: methanol before being loaded onto the LC-MS. MS analysis was conducted on an Exactive orbitrap mass spectrometer (Thermo Fisher Scientific) scanning at 1 Hz and 100,000 resolution operating in negative ion mode. LC separation was on reversed-phase ion-pairing chromatography on a Luna C8 column (150 \times 2.0 mm, 3 μ m particle size, 100 Å pore size; Phenomenex) with a gradient of solvent A (10 mM tributylamine + 15 mM acetic acid in 97:3 water:methanol, pH 4.5) and solvent B (methanol). Flow rate was 250 μ l min⁻¹. The gradient was: 0 min, 80% B; 10 min, 90% B; 11 min, 99% B; 25 min, 99% B; 26 min, 80% B; 30 min, 80% B.

Data availability

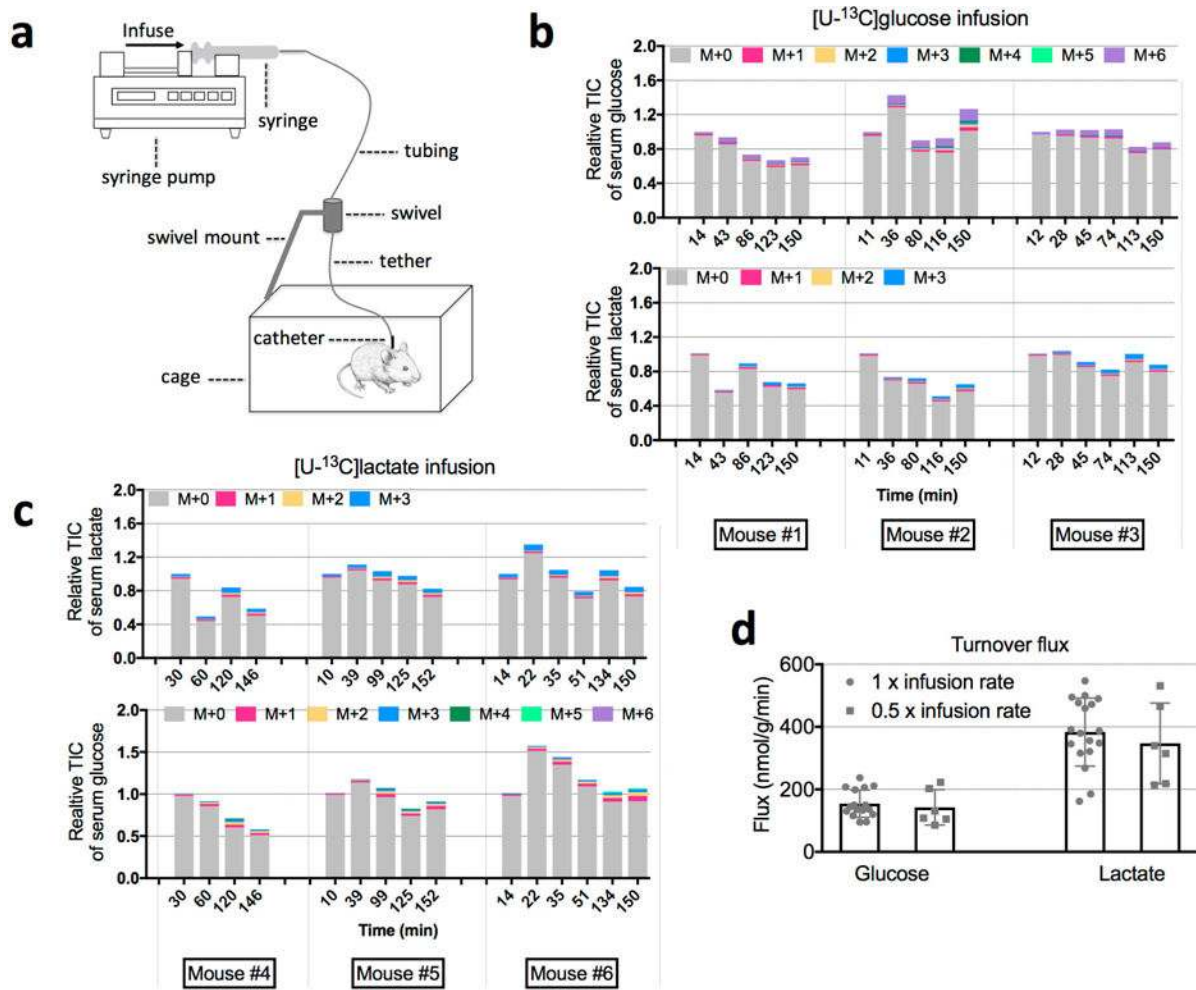
All data are available from the authors upon reasonable request. Source Data for Figs 1b-e, 2a-d, 3a-b and 4a-c and Extended Data Figs 2b-d, 3c, 4a-b, 5a-b, 7a-b, 8a-c and 9a-c are provided with the online version of the paper.

Extended Data



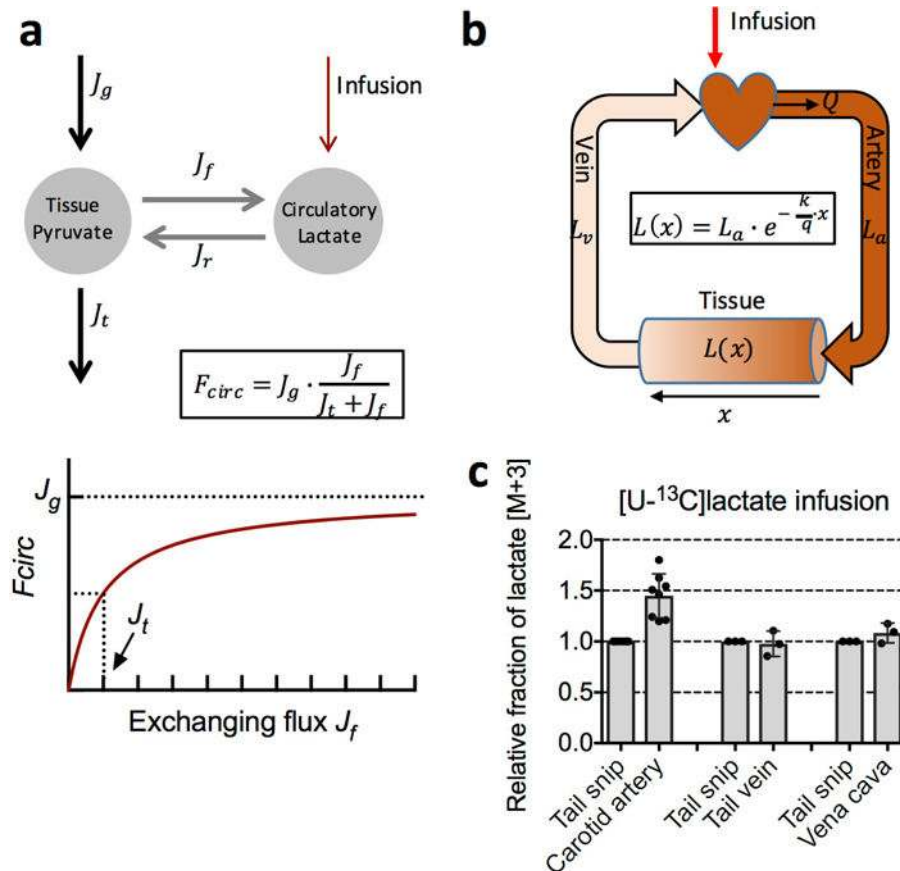
Extended Data Figure 1. Abundant metabolites in mouse plasma

Metabolites ($n = 39$) with reported concentration greater than $30 \mu\text{M}$ in mouse plasma. Left bar graph shows those $> 100 \mu\text{M}$ ($n = 17$) and right bar graph those between $30 \mu\text{M}$ and $100 \mu\text{M}$ ($n = 22$). Most of the data are from the Mouse Multiple Tissue Metabolome Database (<http://mmdb.iab.keio.ac.jp>) ($n = 2$ mice), except for glucose ($n = 6$ mice), acetate ($n = 3$ mice), and glycerol ($n = 3$ mice), whose concentrations were determined in this study. The metabolites shown with red bars ($n = 30$) are those whose turnover fluxes have been determined (Table 1). Values are mean \pm s.d. The concentration cut off of $30 \mu\text{M}$ was calculated using equation (1) where we used a cardiac output of $0.5 \text{ ml g}^{-1} \text{ min}^{-1}$ (see Supplementary Note 1 for references) and a turnover flux equating to 10% of glucose F_{circ} .



Extended Data Figure 2. Determination of turnover flux with isotopic tracing

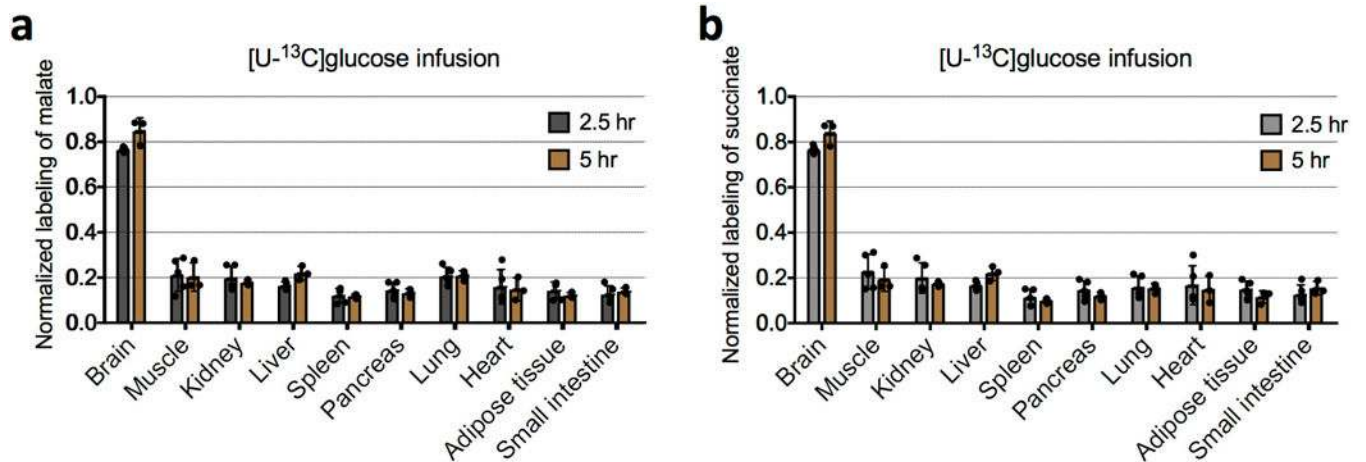
a, Illustration of the mouse infusion experimental setup. **b**, Relative total ion counts (TICs) of serum glucose and lactate during ¹³C-glucose infusion (individual mouse data are shown for three mice for each condition). **c**, Relative TICs of serum glucose and lactate during ¹³C-lactate infusion. **d**, Glucose ($n = 16$ for $1 \times$ and $n = 6$ for $0.5 \times$; $P = 0.61$) and lactate ($n = 18$ for $1 \times$ and $n = 6$ for $0.5 \times$; $P = 0.50$) turnover fluxes determined using two different infusion rates (mean \pm s.d.). P values were determined by a two-tailed unpaired Student's t -test. The $1 \times$ infusion rates are listed in Supplementary Table 1.



Extended Data Figure 3. Measurement of lactate turnover flux

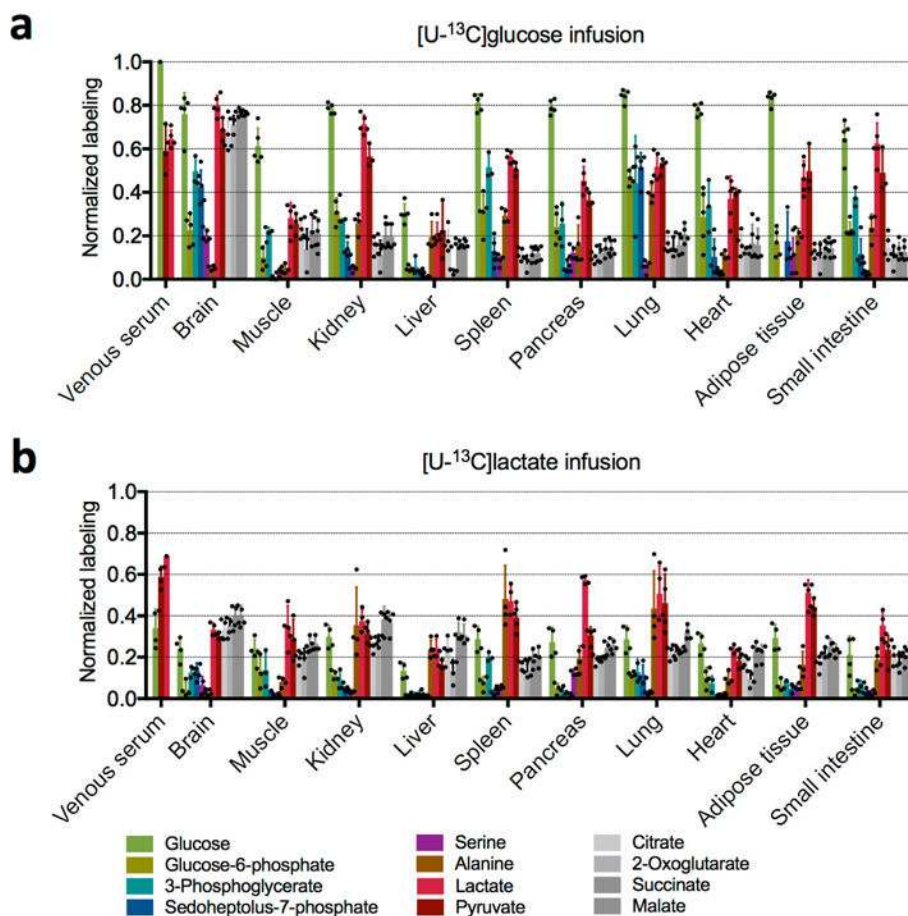
a, The dependence of lactate turnover flux (F_{circ}) on the exchanging flux (forward (J_f) and reverse (J_r)) between circulating lactate and tissue pyruvate. Rapid exchanging flux does not lead to infinitely fast lactate turnover flux. Instead, it leads to a lactate turnover flux approaching the net production rate of pyruvate (J_g), as illustrated in lower panel. J_t is the pyruvate flux going to the TCA cycle. See Supplementary Note 2 for derivation. **b**, Spatial dependence of tracer enrichment. Labelling ($L(x)$) decreases in an exponential manner across a tissue capillary bed (shown schematically in the shading of the cylinder representing tissue) with the extent of arteriovenous difference in tracer labelling depending on the metabolic transformation rate (k) relative to the volumetric blood flow rate ($q = Q/V$; V is tissue volume) as shown in the equation. L_a and L_v are labelled fraction in the artery and the vein, respectively. See Supplementary Note 1. **c**, Lactate labelled fraction in arterial (carotid artery; $n = 8$ mice, mean \pm s.d.) and venous (tail vein and vena cava; $n = 3$ mice, mean \pm s.d.) serum samples, and in tail snip serum sample ($n = 3$ mice, mean \pm s.d.). For comparison of tail snip to vena cava only, samples were collected under anaesthesia to allow access to the inferior vena cava. The difference in lactate labelling between the carotid artery and tail snip can be used to calculate lactate F_{circ} using equation (3). With $Q = 0.53 \pm 0.11$ ml min⁻¹ g⁻¹ and $C = 2.5 \pm 0.2$ mM, together with $\frac{\Delta L}{L_a} \approx 0.3$, we get lactate F_{circ} as 398 ± 88 nmol min⁻¹ g⁻¹ in the fasted state, which is comparable to the value of 374 ± 112 nmol min⁻¹ g⁻¹ obtained with equation (2).

See Supplementary Note 1 for details.



Extended Data Figure 4. Isotopic labelling of tissue TCA intermediates reaches steady state after 2.5-h infusion of ¹³C-glucose

a. Comparison of normalized labelling of tissue malate after 2.5 h ($n = 5$ mice; mean \pm s.d.) and after 5 h of [U-¹³C]glucose infusion ($n = 3$ mice; mean \pm s.d.). P values were determined by an unpaired Student's t -test, corrected for multiple comparisons using the Holm–Sidak method. Normalized labelling is the fraction of ¹³C atoms in a metabolite divided by the fraction of ¹³C atoms in serum glucose. None of the differences are significant ($P > 0.14$ for the brain and liver, and $P > 0.98$ for other tissues). **b.** Comparison of normalized labelling of tissue succinate after 2.5 h ($n = 5$ mice; mean \pm s.d.) and after 5 h of [U-¹³C]glucose infusion ($n = 3$ mice; mean \pm s.d.). None of the differences are significant ($P > 0.18$ for the brain and liver, and $P > 0.85$ for other tissues).

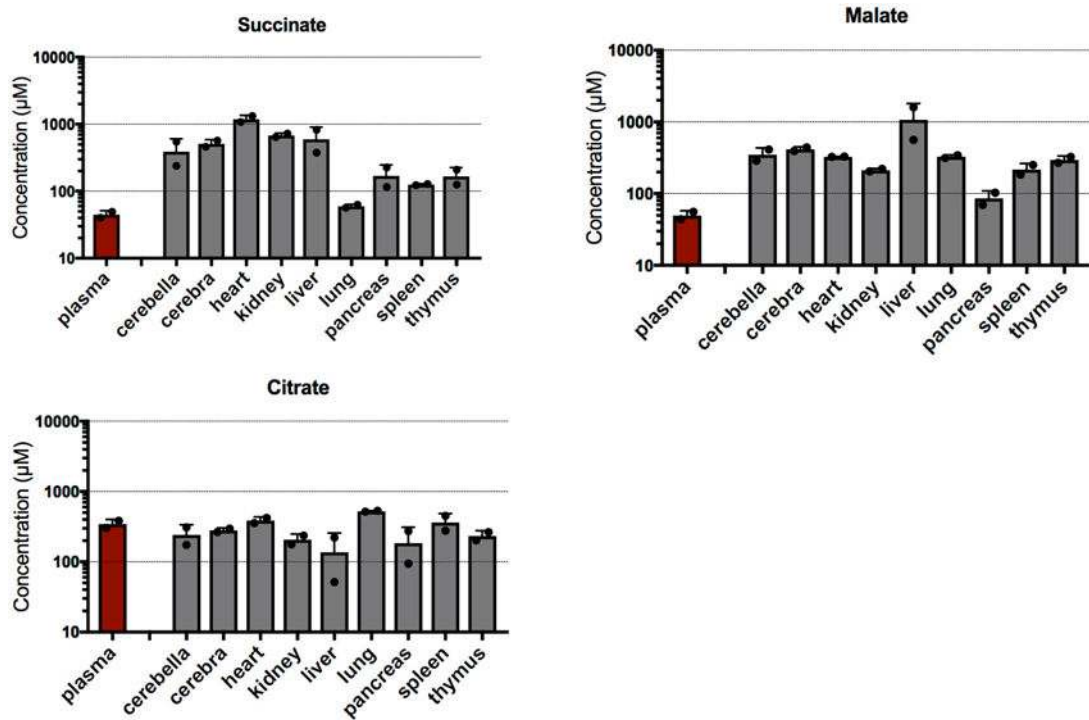


Extended Data Figure 5. Isotope labelling of central carbon metabolites by ^{13}C -glucose and ^{13}C -lactate

a. Normalized labelling by ^{13}C -glucose in fasting mice ($n = 3$ for pyruvate, 2-oxoglutarate, and 3-phosphoglycerate, $n = 4$ for alanine, and $n = 5$ for all other metabolites; mean \pm s.d.).

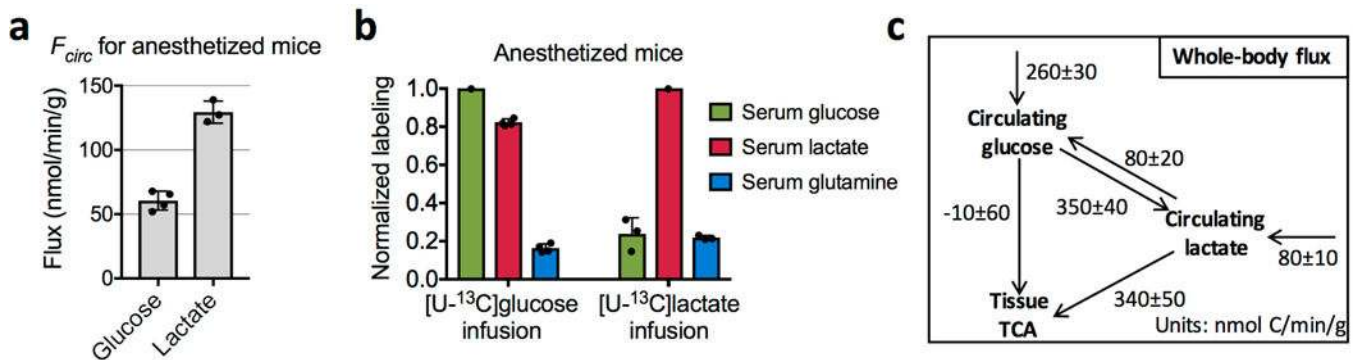
b. Normalized labelling by ^{13}C -lactate in fasting mice ($n = 3$ for 3-phosphoglycerate and $n = 4$ for all other metabolites; mean \pm s.d.). n indicates the number of mice. For the lactate tracer studies, venous serum and tissue labelling are normalized to the arterial serum lactate labelling. Note that citrate, malate and succinate in tissues turn over sufficiently slowly that labelling is robust to the small (<90 s) delay between euthanizing the mouse and tissue harvesting. This delay may, however, result in erroneous measurements for tissue lactate, pyruvate and glycolytic intermediates. Analyses in the main text are limited to the better validated measurements of serum metabolites and tissue TCA intermediates. With this caveat in mind, it is nevertheless intriguing that lactate labelling varies markedly across tissues. After labelled glucose infusion, lactate labelling is highest in the brain, consistent with its use of glucose as a major substrate. In the kidneys lactate is strongly labelled after glucose infusion, even though TCA intermediates are more labelled after lactate infusion. A potential explanation involves tissue heterogeneity; for example, the presence both of glycolytic cells that make lactate from circulating glucose and of oxidative cells that make TCA intermediates from circulating lactate. In other tissues, such as liver, tissue lactate labelling is far below circulating lactate and very similar to TCA labelling; this may reflect

mixing of carbon between lactate and TCA intermediates via gluconeogenesis or pyruvate cycling. Another factor diluting tissue lactate labelling is that, as blood passes through tissue, owing to the rapid exchange between tissue and circulating lactate, the circulating lactate loses its labelling, as is evident from the lactate arteriovenous labelling difference.



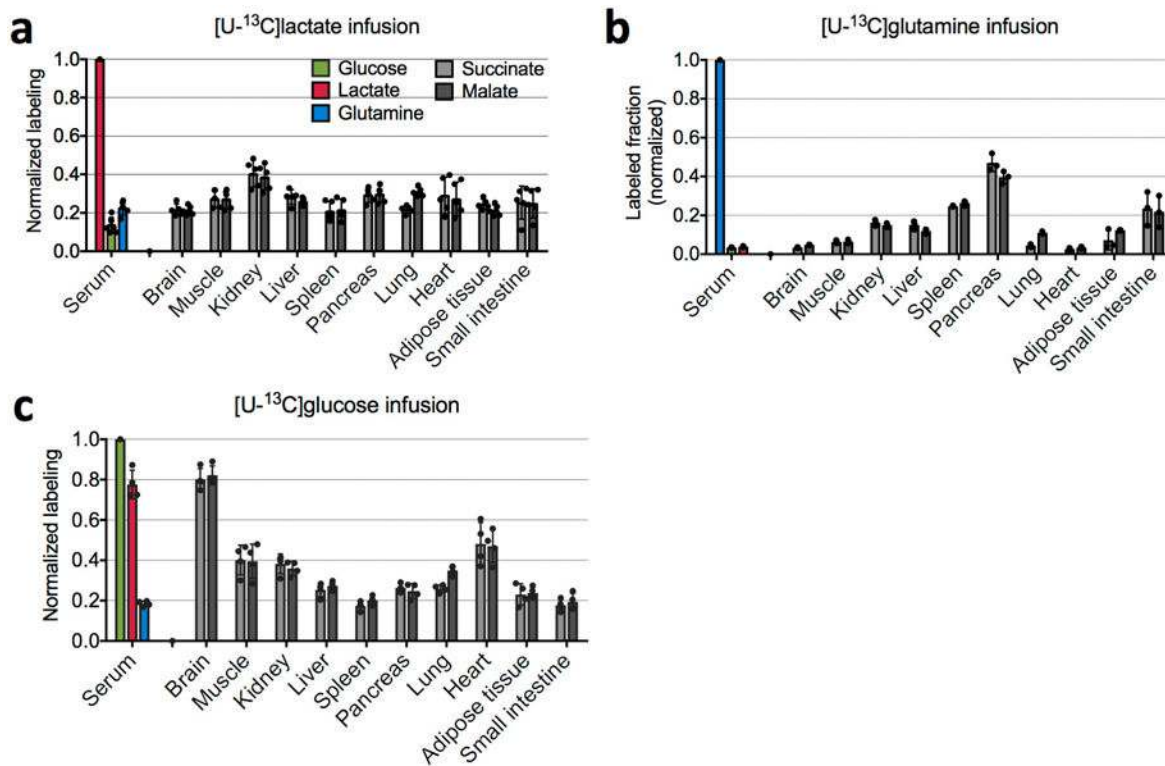
Extended Data Figure 6. Concentrations of succinate, malate, and citrate in mouse plasma and tissues

Unlike citrate, succinate and malate have substantially higher concentrations in tissues than in the bloodstream, thus making them a suitable readout for the tissue TCA cycle. Data are from the Mouse Multiple Tissue Metabolome Database (<http://mmdb.iab.keio.ac.jp>). Values are mean ± s.d. ($n = 2$ mice). Note that the y -axis is a logarithmic scale.

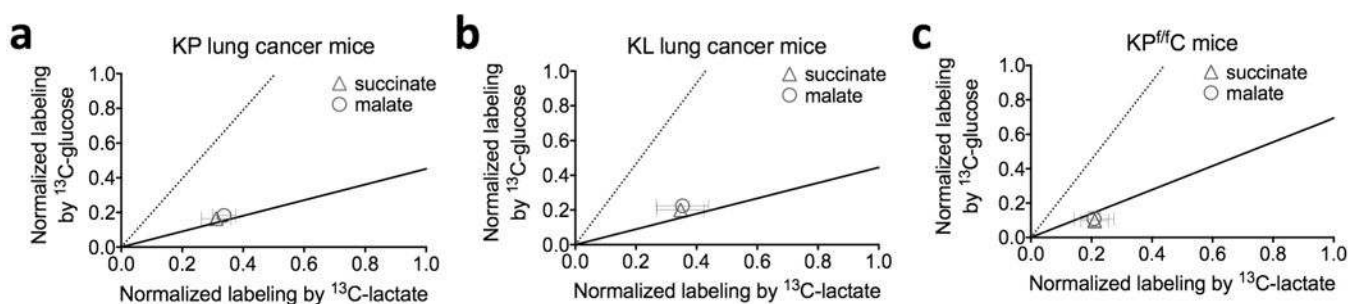


Extended Data Figure 7. Glucose feeds the TCA cycle via circulating lactate in anaesthetized mice

a, Turnover fluxes of glucose ($n = 4$ mice, mean \pm s.d.) and lactate ($n = 3$ mice, mean \pm s.d.) in anaesthetized mice. **b**, Normalized labelling of serum glucose, lactate, and glutamine in anaesthetized mice with ^{13}C -glucose infusion ($n = 4$ mice; mean \pm s.d.) and ^{13}C -lactate infusion ($n = 3$ mice; mean \pm s.d.). **c**, Steady-state whole-body flux model summarizing glucose and lactate interconversion and their feeding to the TCA (see Supplementary Note 4). Values are mean \pm s.e.m.



Extended Data Figure 8. Normalized labelling of serum glutamine, glucose, and lactate, and of tissue TCA intermediates in fed mice
a, ^{13}C -lactate infusion ($n = 5$ mice). **b** ^{13}C -glutamine infusion ($n = 3$ mice). **c**, ^{13}C -glucose infusion ($n = 4$ mice). Bars are mean \pm s.d.



Extended Data Figure 9. Scatter plots of normalized labelling of TCA intermediates in the three types of tumours by ^{13}C -glucose versus that by ^{13}C -lactate
a, $Kras^{LSL-G12D/+}Trp53^{-/-}$ (KP) non-small cell lung cancer ($n = 3$ for ^{13}C -glucose and ^{13}C -lactate infusions, and $n = 4$ for ^{13}C -glutamine infusion). **b**, $Kras^{LSL-G12D/+}Stk11^{-/-}$ (KL)

lung cancer ($n = 3$ mice for infusion of each tracer). **c.** *Kras^{LSL-G12D/+}Trp53^{-/-}Ptf1a^{CRE/+}* (K^{Pf1fC}) pancreatic ductal adenocarcinoma ($n = 4$ for ¹³C-glucose infusion, $n = 3$ for ¹³C-lactate and ¹³C-glutamine infusions). Values are mean \pm s.d. Data are from Fig. 4a–c. The solid line represents the expected labelling by ¹³C-glucose assuming that glucose feeds the TCA cycle solely through circulating lactate. The dashed line indicates the expected labelling by ¹³C-lactate, assuming that lactate feeds the TCA cycle solely through circulating glucose.

Supplementary Material

Refer to Web version on PubMed Central for supplementary material.

Acknowledgments

We thank C. Wright for providing the *Ptf1a-cre* mice; M. Sander for help and advice; and the members of the Rabinowitz laboratory and J. Baur, Z. Arany, and M. Lazar for scientific discussions. This work was supported by NIH grants 1DP1DK113643, R01 CA163591, R01 CA130893, K22 CA190521, R01 CA186043, R35 CA197699, R50 CA211437, P30 CA072720 (Metabolomics Shared Resource, Rutgers Cancer Institute of New Jersey), and 5P30 DK019525. In addition, it was supported by a Stand Up To Cancer-Cancer Research UK-Lustgarten Foundation Pancreatic Cancer Dream Team Research Grant (grant number: SU2C-AACR-DT-20-16). S.H. is a Merck Fellow of the Life Sciences Research Foundation. C.J. is a postdoctoral fellow of the American Diabetes Association.

References

1. van Hall G. Lactate kinetics in human tissues at rest and during exercise. *Acta Physiol (Oxf)*. 2010; 199:499–508. [PubMed: 20345411]
2. Sonveaux P, et al. Targeting lactate-fueled respiration selectively kills hypoxic tumor cells in mice. *J Clin Invest*. 2008; 118:3930–3942. [PubMed: 19033663]
3. Kennedy KM, et al. Catabolism of exogenous lactate reveals it as a legitimate metabolic substrate in breast cancer. *PLoS One*. 2013; 8:e75154. [PubMed: 24069390]
4. Feron O. Pyruvate into lactate and back: from the Warburg effect to symbiotic energy fuel exchange in cancer cells. *Radiother Oncol*. 2009; 92:329–333. [PubMed: 19604589]
5. Hensley CT, et al. Metabolic heterogeneity in human lung tumors. *Cell*. 2016; 164:681–694. [PubMed: 26853473]
6. Sugimoto M, et al. MMMDB: mouse multiple tissue metabolome database. *Nucleic Acids Res*. 2012; 40:D809–D814. [PubMed: 22139941]
7. McCabe BJ, Previs SF. Using isotope tracers to study metabolism: application in mouse models. *Metab Eng*. 2004; 6:25–35. [PubMed: 14734253]
8. Annison EF, Lindsay DB, White RR. Metabolic interrelations of glucose and lactate in sheep. *Biochem J*. 1963; 88:243–248. [PubMed: 14063863]
9. Forbath N, Kenshole AB, Hetenyi G Jr. Turnover of lactic acid in normal and diabetic dogs calculated by two tracer methods. *Am J Physiol*. 1967; 212:1179–1184. [PubMed: 6023874]
10. Searle GL, Cavalieri RR. Determination of lactate kinetics in the human analysis of data from single injection vs. continuous infusion methods. *Proc Soc Exp Biol Med*. 1972; 139:1002–1006. [PubMed: 5023748]
11. Okajima F, Chenoweth M, Rognstad R, Dunn A, Katz J. Metabolism of ³H- and ¹⁴C-labelled lactate in starved rats. *Biochem J*. 1981; 194:525–540. [PubMed: 7306002]
12. Katz J, Okajima F, Chenoweth M, Dunn A. The determination of lactate turnover *in vivo* with ³H- and ¹⁴C-labelled lactate. The significance of sites of tracer administration and sampling. *Biochem J*. 1981; 194:513–524. [PubMed: 7306001]
13. Layman DK, Wolfe RR. Sample site selection for tracer studies applying a unidirectional circulatory approach. *Am J Physiol*. 1987; 253:E173–E178. [PubMed: 3039856]

14. Binder ND, Day D, Battaglia FC, Meschia G, Sparks JW. Role of the circulation in measurement of lactate turnover rate. *J Appl Physiol*. 1991; 70:1469–1476. [PubMed: 2055823]
15. Norwich KH. Sites of infusion and sampling for measurement of rates of production in steady state. *Am J Physiol*. 1992; 263:E817–E822. [PubMed: 1443112]
16. Sacca L, Toffolo G, Cobelli C. V–A and A–V modes in whole body and regional kinetics: domain of validity from a physiological model. *Am J Physiol*. 1992; 263:E597–E606. [PubMed: 1415678]
17. Sauer U. Metabolic networks in motion: ¹³C-based flux analysis. *Mol Syst Biol*. 2006; 2:62. [PubMed: 17102807]
18. Buescher JM, et al. A roadmap for interpreting ¹³C metabolite labeling patterns from cells. *Curr Opin Biotechnol*. 2015; 34:189–201. [PubMed: 25731751]
19. Metallo CM, Walther JL, Stephanopoulos G. Evaluation of ¹³C isotopic tracers for metabolic flux analysis in mammalian cells. *J Biotechnol*. 2009; 144:167–174. [PubMed: 19622376]
20. Warburg O. On the origin of cancer cells. *Science*. 1956; 123:309–314. [PubMed: 13298683]
21. Vander Heiden MG, Cantley LC, Thompson CB. Understanding the Warburg effect: the metabolic requirements of cell proliferation. *Science*. 2009; 324:1029–1033. [PubMed: 19460998]
22. Davidson SM, et al. Environment impacts the metabolic dependencies of Ras-driven non-small cell lung cancer. *Cell Metab*. 2016; 23:517–528. [PubMed: 26853747]
23. Mayers JR, et al. Tissue of origin dictates branched-chain amino acid metabolism in mutant Kras-driven cancers. *Science*. 2016; 353:1161–1165. [PubMed: 27609895]
24. Brooks, G. Circulation, Respiration, and Metabolism. Gilles, R., editor. Springer; 1985. p. 208–218.
25. Whitaker-Menezes D, et al. Evidence for a stromal-epithelial “lactate shuttle” in human tumors: MCT4 is a marker of oxidative stress in cancer-associated fibroblasts. *Cell Cycle*. 2011; 10:1772–1783. [PubMed: 21558814]
26. Brooks GA. Cell-cell and intracellular lactate shuttles. *J Physiol*. 2009; 587:5591–5600. [PubMed: 19805739]
27. Draoui N, Feron O. Lactate shuttles at a glance: from physiological paradigms to anti-cancer treatments. *Dis Model Mech*. 2011; 4:727–732. [PubMed: 22065843]
28. Gladden LB. Lactate metabolism: a new paradigm for the third millennium. *J Physiol*. 2004; 558:5–30. [PubMed: 15131240]
29. Gladden LB. A lactic perspective on metabolism. *Med Sci Sports Exerc*. 2008; 40:477–485. [PubMed: 18379210]
30. Nocito L, et al. The extracellular redox state modulates mitochondrial function, gluconeogenesis, and glycogen synthesis in murine hepatocytes. *PLoS One*. 2015; 10:e0122818. [PubMed: 25816337]
31. Shetty S, et al. Enhanced fatty acid flux triggered by adiponectin overexpression. *Endocrinology*. 2012; 153:113–122. [PubMed: 22045665]
32. Wollenberger A, Ristau O, Schoffa G. Eine einfache Technik der extrem schnellen Abkühlung größerer Gewebestücke. *Pflugers Arch Gesamte Physiol Menschen Tiere*. 1960; 270:399–412.
33. Hingorani SR, et al. Preinvasive and invasive ductal pancreatic cancer and its early detection in the mouse. *Cancer Cell*. 2003; 4:437–450. [PubMed: 14706336]
34. Bardeesy N, et al. Both p16(Ink4a) and the p19(Arf)–p53 pathway constrain progression of pancreatic adenocarcinoma in the mouse. *Proc Natl Acad Sci USA*. 2006; 103:5947–5952. [PubMed: 16585505]
35. Melamud E, Vastag L, Rabinowitz JD. Metabolomic analysis and visualization engine for LC–MS data. *Anal Chem*. 2010; 82:9818–9826. [PubMed: 21049934]
36. Lamarre SG, et al. An isotope-dilution, GC–MS assay for formate and its application to human and animal metabolism. *Amino Acids*. 2014; 46:1885–1891. [PubMed: 24748098]

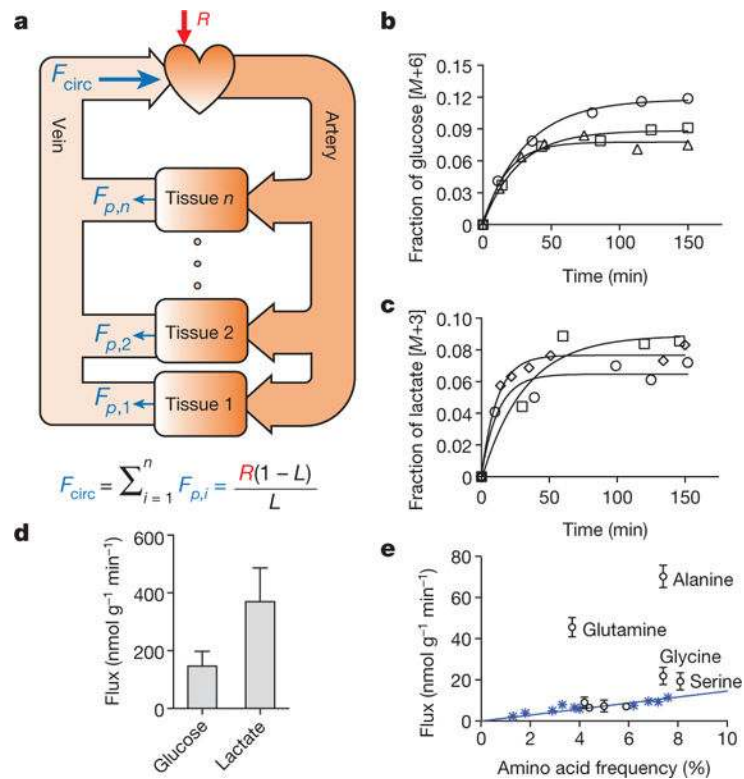


Figure 1. Turnover fluxes of circulating metabolites in fasting mice

a, Illustration of circulatory turnover flux (F_{circ}) and its determination by isotope tracing. **b**, **c**, Kinetics of isotopic labelling of circulating glucose and lactate. Data from different mice are indicated by different symbols and are fitted with a single exponential. **d**, Glucose ($n = 22$) and lactate ($n = 24$) turnover fluxes; data are mean \pm s.d. **e**, Turnover fluxes of amino acids versus their average abundances in mammalian proteins. Blue asterisks, essential amino acids (EAAs). Data are mean \pm s.d.; $n = 5$ for glutamine; $n = 4$ for essential amino acids except tyrosine; $n = 3$ for other amino acids). In all figures, $n =$ number of mice.

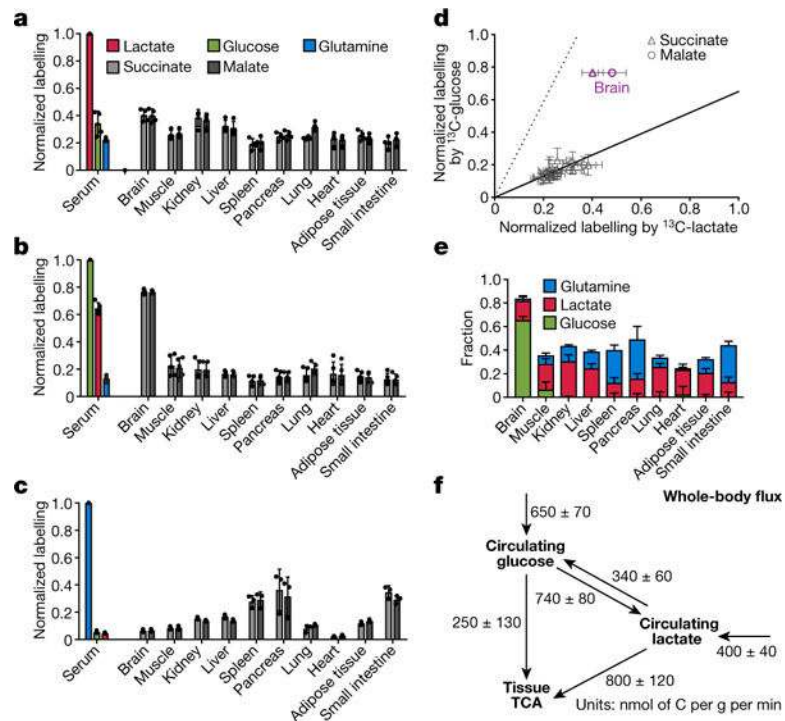


Figure 2. In fasting mice, glucose labels TCA intermediates through circulating lactate in all tissues except the brain

a–c, Normalized labelling of serum glucose, lactate, and glutamine, and of tissue TCA intermediates by infused ^{13}C -lactate (**a**, $n = 4$), ^{13}C -glucose (**b**, $n = 5$), and ^{13}C -glutamine (**c**, $n = 3$). Data are mean \pm s.d. **d**, Scatter plot of normalized labelling of TCA intermediates by infused ^{13}C -glucose versus infused ^{13}C -lactate (^{13}C -glucose and ^{13}C -lactate experiments performed separately). The solid line represents the expected labelling by ^{13}C -glucose assuming that glucose feeds the TCA cycle solely through circulating lactate. The dashed line indicates the expected labelling by ^{13}C -lactate assuming that lactate feeds the TCA cycle solely through circulating glucose. Data are from **a** and **b**, each data point is one TCA intermediate in one tissue, mean \pm s.d., $n = 4$ for ^{13}C -lactate infusion and $n = 5$ for ^{13}C -glucose infusion. **e**, Direct circulating nutrient contributions to tissue TCA cycle (see Supplementary Note 3), data are mean \pm s.e.m. **f**, Steady-state whole-body flux model of interconversion between circulating glucose and lactate and their feeding of TCA (see Supplementary Note 4), data are mean \pm s.e.m.

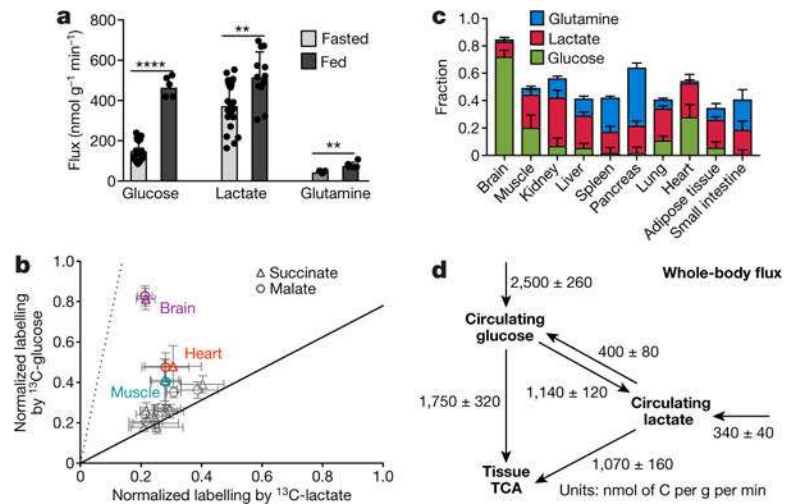


Figure 3. In fed mice, in all tissues except brain and muscle, glucose labels TCA intermediates mostly through circulating lactate

a, Turnover fluxes of glucose, lactate, and glutamine in fed and fasted mice (fed state: $n = 5$ for glucose, $n = 12$ for lactate, and $n = 6$ for glutamine; fasting state: $n = 22$ for glucose, $n = 24$ for lactate, and $n = 5$ for glutamine). Data are mean \pm s.d., **** $P < 0.0001$; ** $P < 0.002$ by t -test. **b**, Normalized labelling of TCA intermediates by ¹³C-glucose versus ¹³C-lactate, as in Fig. 2d, in fed mice. Data are from Extended Data Fig. 8. **c**, Direct circulating nutrient contributions to the tissue TCA cycle in fed mice; data are mean \pm s.e.m. **d**, Steady-state whole-body flux model, as in Fig. 2f, in fed mice; data are mean \pm s.e.m.

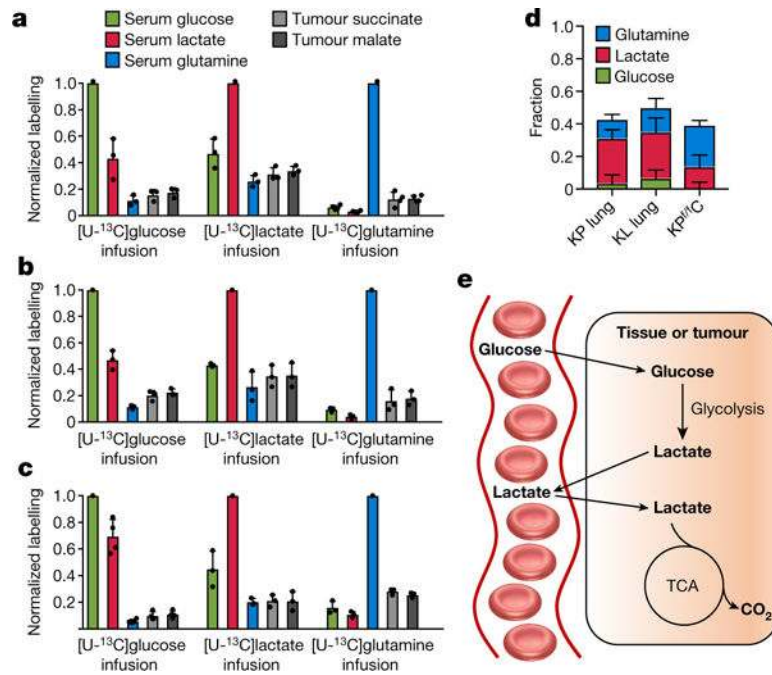


Figure 4. Circulating lactate is a primary TCA substrate in tumours

a–c, Normalized labelling of serum glucose, lactate, and glutamine and of tumour TCA intermediates by infused ¹³C-glucose, ¹³C-lactate, and ¹³C-glutamine in three GEMM tumours in fasted mice. **a**, *Kras^{LSL-G12D/+} Trp53^{-/-}* (KP) lung cancer ($n = 3$ for glucose and lactate and $n = 4$ for glutamine infusion). **b**, *Kras^{G12D/+} Stk11^{-/-}* lung cancer ($n = 3$). *Stk11* is also known as *Lkb1* and the mouse model is called KL lung cancer. **c**, *Kras^{LSL-G12D/+} Trp53^{-/-} Ptf1a^{CRE/+}* (KP^{fl}C) pancreas cancer ($n = 3$ for glucose and $n = 4$ for lactate and glutamine). Data are mean \pm s.d. **d**, Direct circulating nutrient contributions to tumour TCA cycle, data are mean \pm s.e.m. **e**, Schematic representation, glucose feeds the TCA cycle via circulating lactate.

Table 1

Turnover fluxes for different circulating carbon metabolites

Metabolite	F_{circ} (nmol g ⁻¹ min ⁻¹)	Metabolite	F_{circ} (nmol g ⁻¹ min ⁻¹)
Lactate	374.4 ± 112.4	Arginine	9.0 ± 2.6
Glucose	150.9 ± 46.7	Tyrosine	8.0 ± 2.2
Acetate	72.7 ± 17.5	Threonine	7.6 ± 0.8
Alanine	70.2 ± 5.4	Proline	7.3 ± 2.9
Pyruvate	57.3 ± 14.2	Isoleucine	6.5 ± 0.7
Glycerol	53.3 ± 2.1	Asparagine	6.5 ± 0.8
Glutamine	45.6 ± 4.7	Phenylalanine	5.9 ± 0.8
3-Hydroxybutyrate	43.3 ± 17.1	2-Oxoglutarate	5.8 ± 0.8
Palmitic acid	24.6 ± 4.2	Histidine	5.0 ± 0.4
Glycine	21.9 ± 4.2	Methionine	3.9 ± 1.6
Taurine	19.4 ± 0.9	Succinate	3.1 ± 1.1
Serine	19.3 ± 4.2	Creatine	2.6 ± 0.5
Citrate	16.2 ± 6.6	Tryptophan	2.3 ± 0.3
Leucine	11.5 ± 1.2	Malate	2.0 ± 0.4
Valine	9.6 ± 0.4	Betaine	1.6 ± 0.2
Lysine	9.3 ± 1.8		

$n = 24$ for lactate; $n = 22$ for glucose; $n = 5$ for glutamine; $n = 4$ for 3-hydroxybutyrate; $n = 5$ for palmitic acid; $n = 4$ for essential amino acids; $n = 3$ for others; mean ± s.d.